Frontiers of Information Technology & Electronic Engineering
www.jzus.zju.edu.cn; engineering.cae.cn; www.springerlink.com
ISSN 2095-9184 (print); ISSN 2095-9230 (online)
E-mail: jzus@zju.edu.cn

An efficient multi-Bernoulli filter for tracking multiple maritime dim targets*

Liwei SHI, Yunfei GUO†‡, Wenxiong CUI, Yanbo XUE, Yun CHEN

School of Automation, Hangzhou Dianzi University, Hangzhou 310018, China

†E-mail: gyf@hdu.edu.cn

Received May 28, 2024; Revision accepted July 7, 2024; Crosschecked May 13, 2025

Abstract: For the problem of tracking maritime dim targets, the sequential Monte–Carlo multi-Bernoulli track-before-detect (SMC-MB-TBD) method is popular. However, this method may face low tracking accuracy and tracking loss due to particle impoverishment and velocity uncertainty. In this study, a novel filter called position scaling and velocity correction multi-Bernoulli (PSVC-MB) is proposed to deal with this problem. First, particle position scaling is used to replace resampling in the SMC-MB-TBD method to deal with the lack of particle diversity. Second, when the target is stably tracked, the target velocity is extracted from the multi-frame information and used for re-estimation. Pseudo point measurements are calculated from the weighted average of all locations near the particle position, and the particle velocity will be continuously corrected with the pseudo point measurements. Simulation results verify the effectiveness of the proposed method at different low signal-to-clutter ratios (SCRs).

Key words: Maritime dim targets; Track-before-detect; Multi-Bernoulli
https://doi.org/10.1631/FITEE.2400449 **CLC number:** TN953

1 Introduction

Target tracking is usually carried out after setting detection thresholds and compressing observation data into a finite set of point measurements. However, this method may not be suitable in low signal-to-clutter ratio (SCR) situations. A high detection threshold will lead to low detection probability and low yields. Consequently, it is important to use all the information containing the original observation data to improve the tracking performance (Kim et al., 2019).

It is a challenging problem to detect and track dim targets with maritime radar in a complex marine environment. When the radar receives an echo signal generated by the targets, the echo signal will experience interference from the sea clutter, which is reflected from the sea surface (Xu et al., 2021). Sea clutter is not only related to wind speed and surge of the sea surface, but also affected by many factors such as radar parameters and radar operating modes (Posner, 2002). In the case of high resolution, the amplitude of sea clutter has more significant heavy-tail characteristics, and a reasonable sea clutter echo model is K-distribution (Ward et al., 2013).

The track-before-detect (TBD) technique has a wide range of applications in the field of tracking dim targets, and many TBD methods have been proposed so far, mainly including methods based on Hough transform (Moyer et al., 2011), particle filter (PF) (Tian et al., 2022), and dynamic programming (DP) (Yi et al., 2013; Li et al., 2022; Liang et al., 2023). The histogram probabilistic multi-hypothesis tracker (H-PMHT)-based TBD was proposed as an efficient multi-target TBD algorithm (Davey and Gaetjens, 2018; Guo et al., 2023). However, it is found that the calibration of H-PMHT-TBD is difficult in a realistic

‡ Corresponding author
* Project supported by the National Natural Science Foundation of China (Nos. 62371173, U22A2047, and U22A2044) and the Stable Supporting Fund of Acoustic Science and Technology Laboratory (No. JCKYS2024604SSJS009)
ORCID: Yunfei GUO, https://orcid.org/0000-0001-7887-4312

maritime radar setting. The bad calibration leads to poor detection.

Based on the random finite set (RFS) theory, the first multi-target RFS-based TBD algorithm was proposed by Vo et al. (2010). In essence, the key of TBD is to obtain the observational likelihood function that is conjugate to a particular multi-objective distribution. To reduce the numerical complexity, Vo et al. (2010) deduced the analytic features of the corresponding posterior distributions for different prior distributions based on the assumption that the observation regions affected by independent targets do not overlap. Based on the above assumption, the multi-Bernoulli (MB) method is the optimal method of multi-target filtering of TBD data among different prior distributions (Vo et al., 2010). In Papi et al. (2015), the first labeled RFS solution for the multi-target TBD problem was presented under the assumption that the targets do not overlap. Although the separable approximation hypothesis simplifies the filters, the above algorithms have biased estimates when the targets are close. Kim et al. (2021) examined the problem of multi-target tracking in the maritime environment using an MB-TBD filter. In this method, the measurement model evolves into a more general cumulative superposition model to solve the problem when the targets are in close proximity. Ristic et al. (2022) investigated the potential benefits of coherent radar processing and exploitation of Doppler information in the TBD method.

The sequential Monte–Carlo (SMC) method was adopted to implement the MB-TBD filter in Vo et al. (2010). In this algorithm, resampling is used to prevent particle degeneracy after SMC prediction and updating. However, this easily leads to sample impoverishment, which may cause low tracking accuracy and tracking loss (Ristic et al., 2004). In addition, the particle weight is affected only by the particle position, which may lead to the problem that the velocities of heavy particles are not reliable. The heavy particles will be significantly retained in the iteration. Then, in the MB-TBD filter, the existence probability will gradually drop below the threshold to determine the disappearance of the tracked target, which results in tracking loss.

The position scaling and velocity correction multi-Bernoulli (PSVC-MB) filter is proposed in this paper. The main contributions of this paper are as follows:

1. Particle position scaling. The particle position scaling algorithm is proposed to replace the resampling step after SMC-MB updating. According to the scaling angle and the existence probability of the particle sample set, the position of each particle in this set will be scaled, which simultaneously reduces the effects of degeneracy and avoids the loss of diversity.

2. Velocity correction and re-estimation. The particle velocity will be corrected after the particle position scaling step. According to the surviving particle set, pseudo point measurements will be calculated from the weighted average of all locations near the particle position, and the pseudo point measurements are used to update the particle velocity. In addition, when the new-born target is detected steadily, the track re-estimation algorithm will be used for the new-born target individually, which makes the trajectory smooth.

2 Problem formulation

2.1 Target motion model

In a multi-target system, the multi-target state at time k can be naturally represented as a finite subset X_k. If there are N_k targets at time k with states $\boldsymbol{x}_{k,1}$, $\boldsymbol{x}_{k,2}$, $\cdots$, $\boldsymbol{x}_{k,N_k}$, then $X_k = \{\boldsymbol{x}_{k,1}, \boldsymbol{x}_{k,2}, \cdots, \boldsymbol{x}_{k,N_k}\}$ is the multi-target state. For convenience, without designating a specific target, the single target state is represented as $\boldsymbol{x}_k$. Each single target state contains the target position (x_k, y_k), velocity $(\dot{x}_k, \dot{y}_k)$, and echo intensity I_k, as follows:

$$\boldsymbol{x}_k = \left[x_k, \dot{x}_k, y_k, \dot{y}_k, I_k\right]^{\mathrm{T}}. \tag{1}$$

The single target is assumed to move with a constant velocity (CV) model as

$$\boldsymbol{x}_{k+1} = \boldsymbol{F}\boldsymbol{x}_k + \boldsymbol{w}_k. \tag{2}$$

The target state transition matrix is $\boldsymbol{F} = \mathrm{diag}\{\boldsymbol{F}_{\mathrm{m}}, 1\}$, where $\mathrm{diag}\{\cdot\}$ is a function representing a diagonal matrix, and $\boldsymbol{F}_{\mathrm{m}}$ is the state transition matrix, given as follows:

$$\boldsymbol{F}_{\mathrm{m}} = \boldsymbol{E}_2 \otimes \begin{bmatrix} 1 & T \\ 0 & 1 \end{bmatrix}. \tag{3}$$

Here, $\boldsymbol{E}_n$ is the identity matrix of dimension n, $\otimes$ is the Kronecker product, and T is the sampling

interval. $\boldsymbol{w}_k$ is a zero-mean white Gaussian noise with covariance matrix $\boldsymbol{Q}$. The covariance matrix is $\boldsymbol{Q}=\mathrm{diag}\{\boldsymbol{Q}_{\mathrm{m}}, q_{\mathrm{i}}T\}$, where $\boldsymbol{Q}_{\mathrm{m}}$ is the process noise covariance matrix and is given as follows:

$$\boldsymbol{Q}_{\mathrm{m}}=q_{\mathrm{m}}\boldsymbol{E}_2\otimes\begin{bmatrix}T^3/3 & T^2/2\\ T^2/2 & T\end{bmatrix}. \tag{4}$$

Here, q_{i} and q_{m} are the power spectral densities in the amplitude and spatial dimensions, respectively.

2.2 Observation model

The measurement images are obtained by the airborne maritime radar. Assume that the range–azimuth at the center of each resolution cell can be converted to a Cartesian coordinate system based on an unbiased measurement conversion method (Davey and Rutten, 2007). The measured value in resolution cell (i,j) at time k is represented as $z_k^{(i,j)}$, where $i=1,2,...,\alpha$, $j=1,2,...,\beta$, and α and β are the numbers of range cells and azimuth cells, respectively.

When several targets exist at the same time, the measured amplitude in the resolution cell (i,j) at time k is a sum of contributions from each target and the sea clutter. When no target exists, the measured amplitude is affected only by the sea clutter (Vu et al., 2013):

$$z_k^{(i,j)}=\begin{cases}\sum\limits_{n=1}^{N_k}h_{k,n}^{(i,j)}(\boldsymbol{x}_{k,n})+v_k^{(i,j)}, & \text{if targets exist,}\\ v_k^{(i,j)}, & \text{if no target exists,}\end{cases} \tag{5}$$

where $h_{k,n}^{(i,j)}(\cdot)$ is the contribution of the n^{th} target in cell (i,j) at time k, and $v_k^{(i,j)}$ is the contribution of the sea clutter in cell (i,j) at time k.

$h_{k,n}^{(i,j)}(\cdot)$ is called the point spread function (PSF) affected by the target state, given by

$$\begin{aligned}&h_{k,n}^{(i,j)}(\boldsymbol{x}_{k,n})\\ \approx&\frac{I_{k,n}\Delta_x\Delta_y}{2\pi\Sigma^2}\exp\left(-\frac{(i\Delta_x-x_{k,n})^2+(j\Delta_y-y_{k,n})^2}{2\Sigma^2}\right),\end{aligned} \tag{6}$$

where $I_{k,n}$ is the echo intensity of the n^{th} target, Δ_x and Δ_y are the sizes of each resolution cell, Σ is the blurring factor, and $x_{k,n}$ and $y_{k,n}$ are the positions of the n^{th} target. The image affected by the target is finite. When the target is away from the corresponding cell, the cell value approaches zero. Fig. 1 illustrates the schematic of the target influence area.

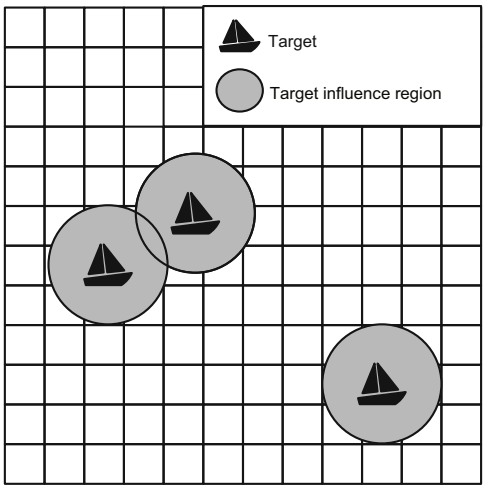

Fig. 1 Schematic of the target influence region

The amplitude of the sea clutter has a significant heavy-tail characteristic, and the reasonable sea clutter echo model is K-distribution. The probability density function (PDF) modeled with K-distribution is given by

$$p_0\left(v_k^{(i,j)}\right)=\frac{4\left(v_k^{(i,j)}\right)^{\rho}}{b^{(\rho+1)/2}\Gamma(\rho)}\kappa_{\rho-1}\left(\frac{2v_k^{(i,j)}}{\sqrt{b}}\right), \tag{7}$$

where ρ and b are the shape parameter and the scale parameter, respectively. $\Gamma(\cdot)$ stands for the gamma function, and $\kappa_{\rho-1}(\cdot)$ refers to the second kind of $(\rho-1)^{\mathrm{th}}$-order modified Bessel function.

Under the K-distribution hypothesis model, the PDF of amplitude contributed by targets and the sea clutter is given below (Ristic et al., 2022):

$$\begin{aligned}&p_1\left(z_k^{(i,j)}\middle|\sum_{n=1}^{N_k}h_{k,n}^{(i,j)}(\boldsymbol{x}_{k,n}),\rho,b\right)\\ =&\int_0^{\infty}\mathrm{Ray}\left(z_k^{(i,j)}\middle|\sum_{n=1}^{N_k}h_{k,n}^{(i,j)}(\boldsymbol{x}_{k,n})\right)\Gamma(\eta\,|\rho,b)\,\mathrm{d}\eta\\ =&\frac{2z_k^{(i,j)}}{b^{\rho}\Gamma(\rho)}\int_0^{\infty}\frac{\eta^{\rho-1}}{\eta+\sum\limits_{n=1}^{N_k}h_{k,n}^{(i,j)}(\boldsymbol{x}_{k,n})}\\ &\cdot\exp\left[-\frac{\eta}{b}-\frac{\left(z_k^{(i,j)}\right)^2}{\eta+\sum\limits_{n=1}^{N_k}h_{k,n}^{(i,j)}(\boldsymbol{x}_{k,n})}\right]\mathrm{d}\eta,\end{aligned} \tag{8}$$

where $\mathrm{Ray}(\cdot)$ is the Rayleigh distribution, and η is the parameter of the Rayleigh distribution representing the power of the background.

The likelihood ratio is defined as

$$\ell\left(z_k^{(i,j)}|\boldsymbol{x}\right)=\frac{p_1\left(z_k^{(i,j)}|\boldsymbol{x}\right)}{p_0\left(z_k^{(i,j)}\right)}. \tag{9}$$

If no target exists, the contribution from targets is equal to 0, i.e., $p_1(\cdot)=p_0(\cdot)$. Hence, the likelihood ratio is equal to 1. The likelihood ratio will be used in Section 3 to update the existence probability.

3 PSVC-MB-TBD

In this section, an algorithm called PSVC-MB-TBD is described to track maritime dim targets. Fig. 2 illustrates the PSVC-MB-TBD flowchart. The proposed algorithm consists of the following five steps: pre-processing, track prediction, track updating, particle position scaling, and velocity correction and re-estimation.

3.1 Pre-processing

3.1.1 K-distribution parameter estimation

The K-distribution parameters are unknown in advance. A method of moment estimator (ME) is used to estimate parameters (Abraham and Lyons, 2002). Weighing up the performance and computational complexity, the estimator employs the first two moments. We regard the measured amplitudes in the resolution cells as the samples $S_1, S_2, ..., S_n$, where n is the number of samples, and the first two moments are defined as

$$m_1=\frac{1}{n}\sum_{i=1}^{n}S_i, \tag{10}$$

$$m_2=\frac{1}{n}\sum_{i=1}^{n}S_i^2. \tag{11}$$

To estimate the K-distribution parameters accurately, the amplitudes of resolution cells at the current moment and the previous frames are taken as samples. The number of samples depends on the size of the K-distribution parameter (Ristic et al., 2020). According to Abraham and Lyons (2002), the parameters ρ and b are obtained as

$$\hat{\rho}\approx\frac{1}{4}\left[\ln\left(\frac{\pi m_2}{4m_1^2}\right)\right]^{-1}, \tag{12}$$

$$\hat{b}=\frac{m_2}{\hat{\rho}}. \tag{13}$$

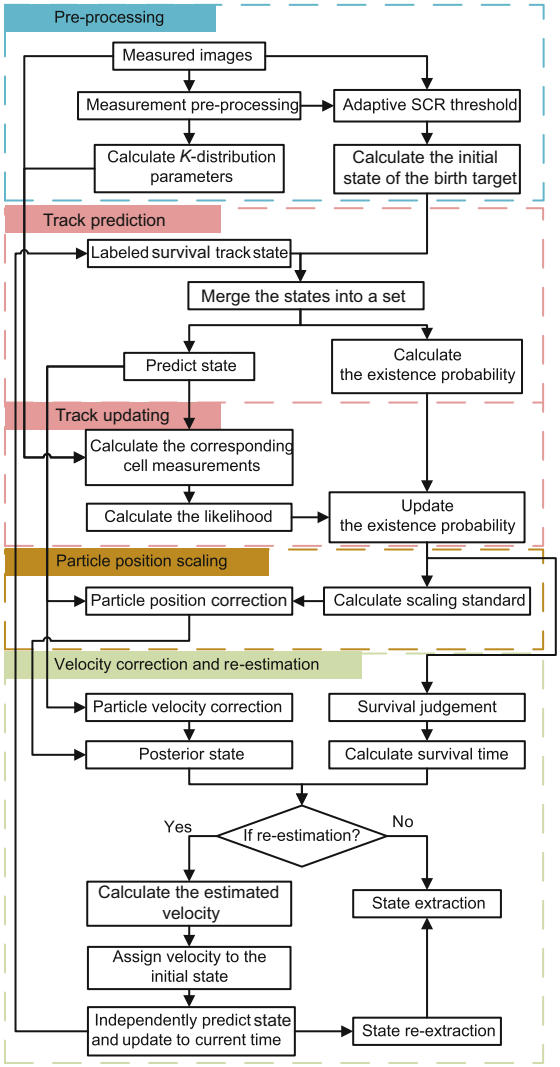

Fig. 2 Flowchart of PSVC-MB-TBD

The estimated parameters $\hat{\rho}$ and $\hat{b}$ are used in the track updating step to calculate the likelihood ratio.

3.1.2 Adaptive SCR threshold

In the low SCR condition, it is difficult to identify the target echo signal from the sea clutter. To balance false alarms and missed detection, an adaptive SCR threshold is set in this study. SCR is defined as

$$\mathrm{SCR}=10\lg\left(\frac{I_k\Delta_x\Delta_y/(2\pi\Sigma^2)}{\sigma_\mathrm{c}}\right)^2, \tag{14}$$

where σ_c is the standard deviation of the sea clutter obeying K-distribution (Davey and Rutten, 2007).

The threshold adopted is shown as follows

(Armstrong and Griffiths, 1991):

$$z_k^{(i,j)} \geq \sqrt{10^{\mathrm{SCR}/10}} \cdot \mathrm{std}(Z_k) + \lambda \cdot \mathrm{mean}(Z_k), \quad (15)$$

where Z_k is the measurement set at time k, and $\mathrm{mean}(\cdot)$ and $\mathrm{std}(\cdot)$ are the mean value function and the standard deviation function, respectively. λ is the proportionality coefficient.

3.2 Track prediction and track updating

The MB filter is a probability density approximation of multi-target Bayesian recursion, which can simultaneously estimate the number of targets and the state. The MB filter can be divided into two steps: prediction and updating.

3.2.1 Prediction

Assume that the multi-target posterior density at time $k-1$ is the MB distribution. An MB RFS can be described by the MB parameter set as follows (Vo et al., 2010):

$$\pi_{k-1} = \left\{ \left(l_{k-1}^{(i)}, r_{k-1}^{(i)}, p_{k-1}^{(i)} \right) \right\}_{i=1}^{N_{k-1}}, \quad (16)$$

where N_{k-1} is the number of targets at time $k-1$, and $r_{k-1}^{(i)}$ and $p_{k-1}^{(i)}$ are the existence probability and the probability density of state of the i^{th} target, respectively. $l_{k-1}^{(i)}$ is the label of the i^{th} target, which contains the birth moment and identification.

The algorithm used in this study is the MB algorithm, which is different from the labeled multi-Bernoulli (LMB) algorithm in Reuter et al. (2014). The labels used in this study include only the birth time and serial number, and each independent Bernoulli component is assigned a unique label to distinguish the track. The labels used in this study are different from the standard expression form; the labels do not take the association of targets and measurements into account. Based on the particularity of the TBD algorithm, a simple tracking label transfer strategy is implemented in this study. That is, when the survival target survives the next frame, the original label is retained for the survival target, and the birth target is assigned a new label. The use of labels in the MB algorithm can be referred to Ristic et al. (2020) and Kim et al. (2021).

Then the predicted multi-target density can be expressed by the following parameter set:

$$\begin{aligned} \pi_{k|k-1} = &\left\{ (l_{\mathrm{s},k|k-1}^{(i)}, r_{\mathrm{s},k|k-1}^{(i)}, p_{\mathrm{s},k|k-1}^{(i)}) \right\}_{i=1}^{N_{k-1}} \\ &\cup \left\{ (l_{\mathrm{b},k}^{(i)}, r_{\mathrm{b},k}^{(i)}, p_{\mathrm{b},k}^{(i)}) \right\}_{i=1}^{N_{\mathrm{b},k}}, \end{aligned} \quad (17)$$

where

$$r_{\mathrm{s},k|k-1}^{(i)} = r_{k-1}^{(i)} \left\langle p_{k-1}^{(i)}, P_{\mathrm{s},k} \right\rangle, \quad (18)$$

$$p_{\mathrm{s},k|k-1}^{(i)}(\boldsymbol{x}) = \frac{\left\langle f_{k|k-1}(\boldsymbol{x}|\cdot), p_{k-1}^{(i)} P_{\mathrm{s},k} \right\rangle}{\left\langle p_{k-1}^{(i)}, P_{\mathrm{s},k} \right\rangle}, \quad (19)$$

$$l_{\mathrm{s},k|k-1}^{(i)} = l_{k-1}^{(i)}, \quad (20)$$

and $N_{\mathrm{b},k}$ is the number of birth targets at time k.

The predicted multi-target density is a combination of survival targets and birth targets. $P_{\mathrm{s},k}$ is the probability of survival. $f_{k|k-1}(\boldsymbol{x}|\cdot)$ is the transfer function. $\langle A, B \rangle \triangleq \int A(x)B(x)\mathrm{d}x$. The label of the survival targets $l_{\mathrm{s},k|k-1}^{(i)}$ inherits the former label. $\left\{ (l_{\mathrm{b},k}^{(i)}, r_{\mathrm{b},k}^{(i)}, p_{\mathrm{b},k}^{(i)}) \right\}_{i=1}^{N_{\mathrm{b},k}}$ is the MB parameter set of the birth targets, in which birth targets are assigned a new label.

3.2.2 Updating

After combining the survival targets and the birth targets, the predicted multi-target density can be expressed as follows:

$$\pi_{k|k-1} = \left\{ (l_{k|k-1}^{(i)}, r_{k|k-1}^{(i)}, p_{k|k-1}^{(i)}) \right\}_{i=1}^{N_{k|k-1}}, \quad (21)$$

where

$$N_{k|k-1} = N_{k-1} + N_{\mathrm{b},k}. \quad (22)$$

Then the updated density at time k can be expressed as follows:

$$\pi_k = \left\{ \left(l_k^{(i)}, r_k^{(i)}, p_k^{(i)} \right) \right\}_{i=1}^{N_k}, \quad (23)$$

where

$$r_k^{(i)} = \frac{r_{k|k-1}^{(i)} \left\langle p_{k|k-1}^{(i)}, \ell\left(Z_k|\boldsymbol{x}\right) \right\rangle}{1 - r_{k|k-1}^{(i)} + r_{k|k-1}^{(i)} \left\langle p_{k|k-1}^{(i)}, \ell\left(Z_k|\boldsymbol{x}\right) \right\rangle}, \quad (24)$$

$$p_k^{(i)} = \frac{p_{k|k-1}^{(i)} \ell\left(Z_k|\boldsymbol{x}\right)}{\left\langle p_{k|k-1}^{(i)}, \ell\left(Z_k|\boldsymbol{x}\right) \right\rangle}, \quad (25)$$

$$\ell\left(Z_k|\boldsymbol{x}\right) = \prod_{(i,j)\in R(\boldsymbol{x})} \ell\left(z_k^{(i,j)}|\boldsymbol{x}\right), \quad (26)$$

$$N_k = \sum_{i=1}^{N_{k|k-1}} \varepsilon\left(r_k^{(i)}\right), \tag{27}$$

$$\varepsilon(x) = \begin{cases} 1, & x \geq r_\mathrm{s}, \\ 0, & x < r_\mathrm{s}. \end{cases} \tag{28}$$

$R(\boldsymbol{x})$ is the target influence area. All the $N_{k|k-1}$ candidate tracks are updated. Only the targets whose existence probability is larger than the survival threshold r_s are preserved for iterative calculation with the corresponding label.

3.3 Particle position scaling

In this subsection, we discuss our proposed particle position scaling method to replace the resampling method. In the proposed method, the low-weight particles are given the opportunity to move closer to the high-weight particles. In the updating step, the weight of each particle is calculated according to the particle state and measurements. The higher the particle measurement likelihood, the greater the particle weight. After the updating step, the resampling method is used by the SMC-MB-TBD algorithm to achieve survival of the fittest. Particles with high weight are retained in large numbers, and deletion of particles with low weight is very probable. The resampling method ignores the potentiality of low-weight particles. According to the resampling method theory (Ristic et al., 2004), a relatively moderate method is adopted in this study. In this method, the low-weight particles will not be completely removed, and are given a chance to be retained, but currently, these low-weight particles must compromise, and get closer to the higher-weight particles. The closer these low-weight particles are to the maximum-weight particle, the higher the measurement likelihood calculated from the states of the low-weight particles. Then these particles will have a greater advantage at the next updating step.

The two main reasons for particle degeneracy are as follows:

1. Particles are affected by the measurement noise; sometimes the particle weights close to the true state are low, but the weights of particles with wrong states are high. Low-weight particles whose states are close to the true state are deleted.

2. Frequent resampling results in a decrease in the particle diversity. The proposed method does not delete the low-weight particles, and unlike the resampling method, this method does not retain a large number of the same particles. Therefore, the particle position scaling method reduces the effects of particle degeneracy.

The parameter scaling angle and existence probability are used to limit the speed of particle movement, and the density detector method is proposed to prevent the particle sample set from being too dense. Fig. 3 illustrates the difference between the resampling and the particle position scaling methods.

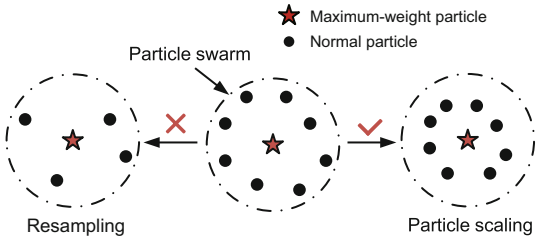

Fig. 3 Schematic of the resampling method and the particle scaling method

3.3.1 Particle position scaling theory

For convenience, this subsection does not index the number of targets. Assume that a particle sample set at time k can be represented as $\left\{(\boldsymbol{x}_k^{(i)}, \omega_k^{(i)})\right\}_{i=1}^{M_\mathrm{p}}$.

A particle sample set consists of M_p particles, and each particle can be described by its state $\boldsymbol{x}_k$ and weight ω_k.

After the updating step, the particle will move toward the maximum-weight particle according to the scaling angle and the existence probability. The higher the existence probability of the particle sample set is, the closer the particle will be to the maximum-weight particle. Fig. 4 shows a schematic of the particle scaling algorithm.

$$x_{k\_\mathrm{new}}^{(i)} = x_k^{(i)} + (1 - \cos(r_k\theta))(x_k^{\omega\_\max} - x_k^{(i)}), \tag{29}$$

where $x_{k\_\mathrm{new}}^{(i)}$ is the position of the i^{th} particle after position scaling, and $x_k^{\omega\_\max}$ is the position of the maximum-weight particle. r_k is the existence probability of the targets, and θ is the scaling angle.

$y_{k\_\mathrm{new}}^{(i)}$ and $y_k^{\omega\_\max}$ are the counterparts of $x_{k\_\mathrm{new}}^{(i)}$ and $x_k^{\omega\_\max}$ on the y axis, respectively.

To ensure that all the particles are equal in the next updating step, the weight of each particle will be equally distributed as follows:

$$\omega_k^{(i)} = \frac{1}{M_\mathrm{p}}. \tag{30}$$

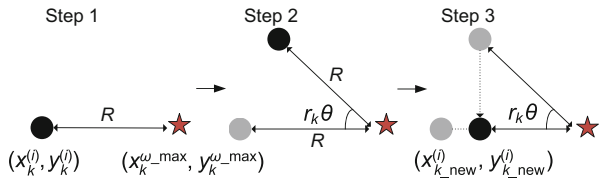

Fig. 4 Schematic of the particle scaling algorithm

3.3.2 Density detector

The particles of the sample set will gradually approach the maximum-weight particle without limitation. The density of the particle sample set will be larger, which leads to a lack of particle diversity. Therefore, the density detector method is used. Fig. 5 shows that when the density is larger than the threshold, the scaling will be stopped and the particles will move freely to ensure particle diversity.

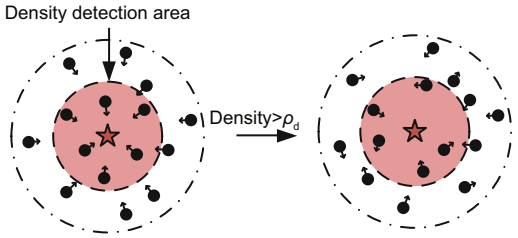

Fig. 5 Density detection to ensure particle diversity

The density ρ_d is calculated as follows:

$$\rho_\mathrm{d} = \sum_{i=1}^{M_\mathrm{p}} D(x_k^{(i)}), \tag{31}$$

where

$$D(x_k) = \begin{cases} 1, & \left|x_k, x_k^{\omega\_\max}\right| \le d, \\ 0, & \left|x_k, x_k^{\omega\_\max}\right| > d. \end{cases} \tag{32}$$

$\left|x_k, x_k^{\omega\_\max}\right|$ is the Euclidean distance between the maximum-weight particle and other particles, and d is the density detector distance. Eq. (32) is used to calculate the density of the particle set. When the density is sufficient, the particle position scaling step will be stopped.

3.4 Velocity correction and re-estimation

The particle sample set of the birth targets at time k is generated according to the measurement z_{k-1}. Because z_{k-1} does not contain information about the target velocity, the particle velocities are distributed in an inaccurate velocity range (Ristic et al., 2020), and the inaccurate velocity of the particle may lead to frequent track breakage. Therefore, a velocity correction and re-estimation method is proposed. Due to the influence of the sea clutter, it is not persuasive to regard the high amplitude resolution cells as point measurements in low SCRs directly. In the proposed method, after the particle position scaling step, the effect of the surviving target in each resolution cell is calculated as a pseudo measurement. In the influence area of the surviving target, the weight of each resolution cell is calculated by multiplying the amplitude of the relative resolution cell by the relative likelihood ratio. Finally, the pseudo point measurement is obtained according to the weight of each resolution cell and used to correct the particle velocity. For a confirmed track, the particle re-estimation method is proposed to extract the velocity. Then the extracted velocity is assigned to the initial state, and the state will be individually re-estimated and synchronized to the present time.

3.4.1 Velocity correction

The pseudo measurements of each resolution cell at time k are calculated according to the surviving particle sample set as follows:

$$d_k^{(i,j)} = \frac{1}{M}\sum_{n=1}^{N}\sum_{c=1}^{M} h_k^{(i,j)}\left(\boldsymbol{x}_k^{(n,c)}\right), \tag{33}$$

where N is the number of the surviving particle sample sets and M is the number of particle samples per set.

Because of the influence of clutter, it is unreliable to determine the weight only by the amplitude, and the weight of each resolution cell is simultaneously affected by the amplitude of the corresponding resolution cell and the pseudo-likelihood ratio, expressed as follows:

$$\omega_k^{(i,j)} = \frac{z_k^{(i,j)} p_1\left(z_k^{(i,j)} | d_k^{(i,j)}\right)}{p_0\left(z_k^{(i,j)}\right)}. \tag{34}$$

Then the pseudo point measurement near the particle position is determined by

$$Z_k^{(n)} = \frac{\sum\limits_{(i,j)\in R(\boldsymbol{x}_k^{(n)})} \omega_k^{(i,j)} C^{(i,j)}}{\sum\limits_{(i,j)\in R(\boldsymbol{x}_k^{(n)})} \omega_k^{(i,j)}}, \tag{35}$$

where $C^{(i,j)}$ is the location of the resolution cell. The final correction velocity is determined by

$$v_k^{(n,c)} \leftarrow v_k^{(n,c)} + (1 - r_k^{(n)})(Z_k^{(n)} - \boldsymbol{x}_k^{(n,c)}), \quad (36)$$

where $r_k^{(n)}$ is the existence probability of the n^{th} surviving target at time k.

The gain of the velocity correction depends on the existence probability. A target with high existence probability is expected to keep the current state for iteration. Therefore, the gain of the velocity correction is low. For the target with low existence probability, the estimated location of the target may be far away from the real location. Therefore, the gain of the velocity correction is expected to be significant to increase the existence probability of the target in the next frame.

3.4.2 Re-estimation

After the updating step, the existence probability $r_k^{(i)}$ of the i^{th} target is calculated. When the existence probability is greater than the survival threshold r_{s}, the target is considered to exist at the current time. The survival time is calculated from the first time the existence probability of the target is greater than the survival threshold. When the survival time of the target is greater than the threshold, the target can be considered to be stably tracked.

Up to time k, according to the effective estimated trajectory and target labels, the corresponding target velocity can be extracted. For simplicity, the target is assumed to move with a CV model, and the velocity is extracted as follows:

$$\overline{v}_x = \frac{\hat{x}_k - \hat{x}_{t_{\text{b}}}}{k - t_{\text{b}}}, \quad (37)$$

where $\hat{x}_k$ is the estimated position in the x axis at time k and t_{b} is the birth moment according to the label.

The extracted velocity is re-assigned to the state of the birth moment, and the state from time t_{b} will be individually re-estimated and synchronized to the present time.

The particle velocity is randomly assigned initially according to the velocity interval, and the velocity of each particle may have a significant difference in direction or size. Without limitation, the particle set used to represent target will be gradually looser. As a result, the trajectory of the target will be more tortuous. The re-estimation method is adopted to estimate the velocity of the target according to the estimated target state and assign the velocity to the particles. Because the velocity direction and size of the particles are roughly similar, the set of particles representing the same target will not become loose due to time. In multiple frames, the target trajectory will be relatively smooth.

3.5 Implementation

The SMC-MB algorithm is used to solve the multi-dimensional integration problem in Eqs. (18), (19), (24), and (25) (Ristic et al., 2013). The probability density of states about the i^{th} target $p_{k-1}^{(i)}$ can be approximated by a particle sample set $\left\{(\boldsymbol{x}_{k-1}^{(i,j)}, \omega_{k-1}^{(i,j)})\right\}_{j=1}^{M_{\text{p}}}$. The predicted density of the surviving target $p_{\text{s},k|k-1}^{(i)}$ is approximated by $\left\{(\boldsymbol{x}_{k|k-1}^{(i,j)}, \omega_{k|k-1}^{(i,j)})\right\}_{j=1}^{M_{\text{p}}}$, where $\boldsymbol{x}_{k|k-1}^{(i,j)} = f_{k|k-1}(\boldsymbol{x}_{k-1}^{(i,j)}|\cdot)$ and $\omega_{k|k-1}^{(i,j)} = P_{\text{s},k}\omega_{k-1}^{(i,j)}$. The selected measurements in Eq. (15) are clustered based on density (Ester et al., 1996), and the optimal measurements are obtained from each cluster by amplitude comparison. The positions of the birth particles are randomly distributed around the optimal measurements. The initial velocities of the birth particles are randomly assigned according to the maximum achievable velocity range. The predicted existence probability is $r_{k|k-1}^{(i)} = r_{k-1}^{(i)} \sum_{j=1}^{M_{\text{p}}} \omega_{k|k-1}^{(i,j)}$. Then the posterior density $p_k^{(i)}$ is approximated by $\left\{(\boldsymbol{x}_{k|k-1}^{(i,j)}, \omega_{k|k}^{(i,j)})\right\}_{j=1}^{M_{\text{p}}}$, where $\omega_{k|k}^{(i,j)} = \ell\left(Z_k|\boldsymbol{x}_{k|k-1}^{(i,j)}\right)\omega_{k|k-1}^{(i,j)}$. The existence probability $r_k^{(i)}$ is calculated as follows:

$$r_k^{(i)} = \frac{r_{k|k-1}^{(i)} \sum_{j=1}^{M_{\text{p}}} \omega_{k|k}^{(i,j)}}{1 - r_{k|k-1}^{(i)} + r_{k|k-1}^{(i)} \sum_{j=1}^{M_{\text{p}}} \omega_{k|k}^{(i,j)}}. \quad (38)$$

After the updating step, the particle scaling method is used to increase the effectiveness of each particle, and avoid the lack of diversity faced by the resampling algorithm. The particle sample set with an existence probability greater than the threshold will be identified as a surviving target and reserved for iteration.

Using the confirmed surviving targets, the

pseudo measurements are calculated to obtain the weight of each resolution cell. The larger the weight, the more likely it is that the amplitude of the corresponding resolution cell is affected by the target. Then pseudo point measurements are calculated around the surviving targets to correct the particle velocity. For each stably tracked target, we can obtain its birth moment based on its label. Targets whose survival time is greater than the threshold will be re-estimated separately by backtracking. The target label processing steps are listed in Algorithm 1.

Algorithm 1 Processing the target labels

for $k=1,2,...,K$ **do**
  for $i=1,2,...,N_{\mathrm{b},k}$ **do**
    Assign labels to the birth targets
    $l_{\mathrm{b},k}^{(i)}=[k,i]$
  end for
  for $j=1,2,...,N_{\mathrm{b},k}+N_{k-1}$ **do**
    Predict $l_{k|k-1}^{(j)}=l_{k-1}^{(j)}$
    Update $l_k^{(j)}=l_{k|k-1}^{(j)}$
  end for
  $N_{k|k-1}=N_{k-1}+N_{\mathrm{b},k}$
  Update the density: $\pi_k=\left\{(l_k^{(i)},r_k^{(i)},p_k^{(i)})\right\}_{i=1}^{N_{k|k-1}}$
  $N_k=0$
  for $i=1,2,...,N_{k|k-1}$ **do**
    if $r_k^{(i)}\geq r_{\mathrm{s}}$ **then**
      Reserve $l_k^{(i)}$, $r_k^{(i)}$, and $p_k^{(i)}$
      $N_k=N_k+1$
    end if
  end for
  The posterior density: $\pi_k=\left\{(l_k^{(i)},r_k^{(i)},p_k^{(i)})\right\}_{i=1}^{N_k}$
end for

The proposed algorithm has a separable form of likelihood measurement based on the assumption that the target influence areas do not overlap. When multiple targets are close to each other, some equations in this study need to be modified. Assume that there are $N_{\mathrm{c},k}$ targets close to each other and $\boldsymbol{x}_m$ is the state of the m^{th} target. When we update the track of target 1, the likelihood ratio needs to be modified as follows:

$$\ell(\bar{z}_k^{(i,j)}|\boldsymbol{x}_1)=\frac{p_1(\bar{z}_k^{(i,j)}|\boldsymbol{x}_1)}{p_0(\bar{z}_k^{(i,j)})},\tag{39}$$

where

$$\bar{z}_k^{(i,j)}=z_k^{(i,j)}-\sum_{m=2}^{N_{\mathrm{c},k}}h_k^{(i,j)}(\boldsymbol{x}_m).\tag{40}$$

When targets are close to each other, the measured amplitude in the resolution cell (i,j) at time k is a sum of contributions from the $N_{\mathrm{c},k}$ targets and the sea clutter. When we update the track of target 1, the contribution from other close targets must be removed.

In addition, the weight of each resolution cell in Eq. (34) needs to be modified as follows:

$$w_k^{(i,j)}=\frac{\bar{z}_k^{(i,j)}p_1(\bar{z}_k^{(i,j)}|d_k^{(i,j)})}{p_0(\bar{z}_k^{(i,j)})}.\tag{41}$$

4 Simulations

In the simulations, the proposed PSVC-MB algorithm is compared with the traditional SMC-MB algorithm and the H-PMHT algorithm to verify the effectiveness of tracking maritime dim targets. Simulations are performed on a personal computer with Intel i5-7400 3.00 GHz central processing unit (CPU), and all the algorithms are implemented in MATLAB R2016a. The particle position scaling method is used instead of the resampling method in this study. The particle position scaling method does not replicate the high-weight particles after the updating step, so the mean squared error and bias in Chesser et al. (2022) are not suitable for evaluation in this study. There are three other indices to evaluate the detection performance: optimal subpattern assignment (OSPA), average number of track losses (ANTL), and average track confirmation delay (ATCD). The three indices are defined as follows:

1. OSPA. This index evaluates the overall performance of the target tracking system, and can be used to measure the error between the real track and the estimated track:

$$\begin{aligned}&\bar{d}_p^{(c)}(X,Y)\\&=\left[\frac{1}{e}\left(\min_{\pi\in\Lambda_e}\sum_{i=1}^{g}d^{(c)}\left(x_i,y_{\pi(i)}\right)^p+c^p(e-g)\right)\right]^{\frac{1}{p}},\end{aligned}\tag{42}$$

where $X=\{x_i\}_{i=1}^{g}$ and $Y=\{y_i\}_{i=1}^{e}$ are arbitrary finite sets of the true target states and the estimated positions with dimensions g and e, respectively. Λ_e represents the set composed of all permutations from 1 to e, and $d^{(c)}(x,y)=\min\{c,d(x,y)\}$, where $d(x,y)=\|x-y\|$, $c>1$, and $1\leq p\leq\infty$.

2. ANTL. This index is used to measure the average variance between the number of true tracks

and the number of estimated tracks:

$$N_{\text{lost}}=\frac{1}{N_{\text{mc}}}\sum_{k=1}^{K}\sum_{i=1}^{N_{\text{mc}}}(N_{k,\text{true}}^{i}-N_{k,\text{est}}^{i}),\qquad(43)$$

where $N_{k,\text{true}}^{i}$ and $N_{k,\text{est}}^{i}$ are the numbers of true tracks and estimated tracks in the i^{th} simulation respectively, and N_{mc} is the number of Monto–Carlo runs.

3. ATCD. This index is used to reflect the sensitivity of target detection:

$$T_{\text{del}}=\frac{1}{N_{\text{mc}}N_{\text{tar}}}\sum_{i=1}^{N_{\text{mc}}}\sum_{j=1}^{N_{\text{tar}}}(T_{\text{b,est}}^{i,j}-T_{\text{b,true}}^{i,j}),\qquad(44)$$

where $T_{\text{b,true}}^{i,j}$ and $T_{\text{b,est}}^{i,j}$ are the true and estimated birth moments of the j^{th} target in the i^{th} simulation, respectively. N_{tar} is the number of targets.

Table 1 shows the scenario and algorithm parameters. The targets are assumed to move with CV models. Each target appears and disappears in the surveillance area at different times. The concrete target parameters are shown in Table 2.

Table 1 Scenario and algorithm parameter setting

Parameter	Symbol and value
Sampling interval	T=1 s
Duration time	K=50 s
Number of Monte–Carlo runs	N_{mc}=50
Numbers of resolution cells	$\alpha=\beta$=65
Sizes of resolution cells	$\Delta_x=\Delta_y$=1 pixel
Sea clutter parameters	$\rho=3,\ b=0.45$
Initial target SCR	SCR=6 dB
Sensor blurring factor	Σ=1
Std of the target location noise	$\sigma_x^{\text{t}}=\sigma_y^{\text{t}}$=0.01 pixels
Survival threshold	r_{s}=0.6
Scaling angle	θ=60°
Density detection distance	d=1.5 pixels
OSPA parameters	$c=5,\ p=1$

Table 2 Concrete target parameter setting

Target index	Survival time (s)	Initial state
1	1–40	[5 pixels, 0.3 pixel/s, 7 pixels, 0.4 pixel/s]
2	10–50	[10 pixels, 0.6 pixel/s, 5 pixels, 0.3 pixel/s]

In the simulation by Vo et al. (2010), the size of pixels is variable. Due to the difference in measurement accuracy and resolution cell size of different sensors, we use pixels to make the unit uniform in this study. The density detection distance in Table 1 is the parameter in Eq. (32). This parameter is used to determine whether the particle position scaling step is required.

Fig. 6 shows the true and estimated tracks with three different algorithms at 6 dB. In Fig. 6, the trajectories obtained by using the traditional SMC-MB algorithm break frequently, because resampling leads to sample impoverishment during iteration, and the velocities of reserved particles are not true, which causes low track accuracy and track loss. The tracking performance of the H-PMHT algorithm is similar to that of the proposed PSVC-MB algorithm. However, obvious track fluctuation occurs with the H-PMHT algorithm, because the relatively high prediction error generally leads to large deviations between the virtual and true measurements in low SCRs.

Fig. 7 shows the OSPA distance of three different algorithms. Fig. 8 shows the estimated number of targets of three different algorithms in 50 Monte–Carlo runs. It can be seen from Figs. 7 and 8 that the H-PMHT algorithm is slower than the proposed algorithm in detecting and tracking targets, because the track confirmation step is required in the H-PMHT algorithm. The average track confirmation time of the H-PMHT algorithm is longer than that of the proposed algorithm.

To verify the effectiveness of the proposed algorithm at a low SCR, 50 Monte–Carlo runs are performed. Fig. 9 shows the average OSPA distance of three algorithms when SCR=4, 6, and 9 dB. Table 3 shows the concrete performance indices of three different algorithms with different SCRs.

Table 3 Performance indices of three algorithms against different SCRs

Index	SCR (dB)	SMC-MB	H-PMHT	PSVC-MB
OSPA	4	3.765	3.573	1.435
	6	2.135	2.282	1.139
	9	1.666	1.768	0.614
ANTL	4	14.15	10.60	9.55
	6	9.02	7.80	3.04
	9	7.83	5.86	2.91
ATCD	4	4.95	8.10	4.85
	6	2.05	5.05	1.90
	9	1.05	2.75	0.95

When the updated particles are looser, the particle position scaling step in the proposed algorithm makes the particles more compact. However, when

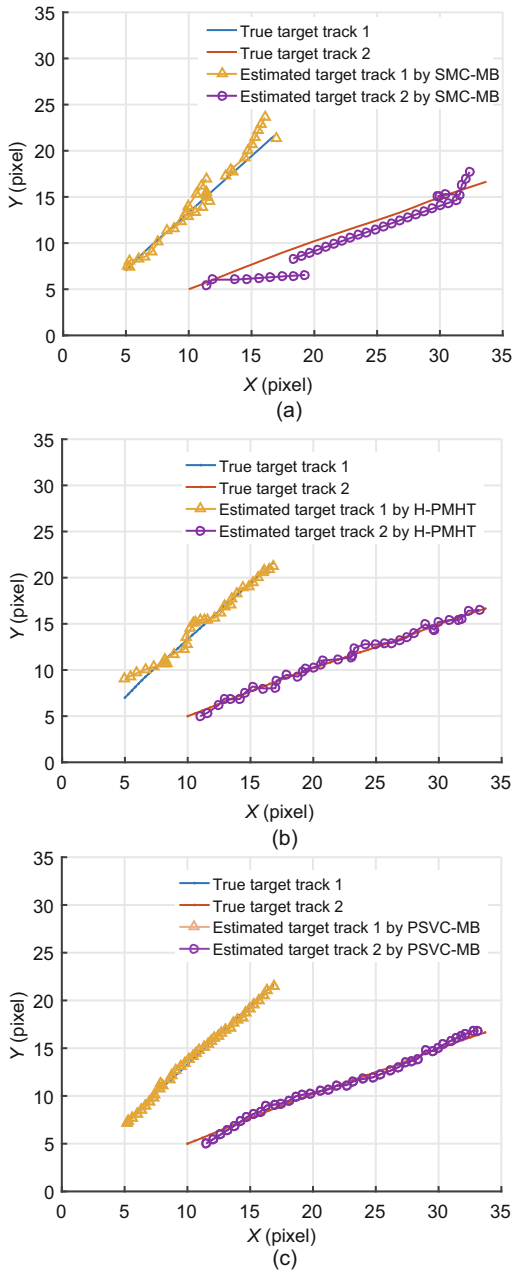

Fig. 6 Target tracks of three different algorithms at 6 dB: (a) SMC-MB; (b) H-PMHT; (c) PSVC-MB

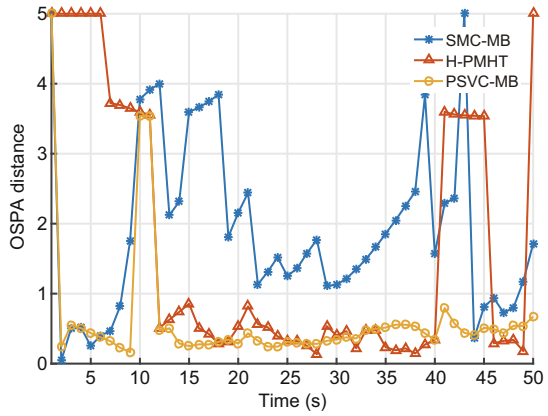

Fig. 7 OSPA distance of three different algorithms

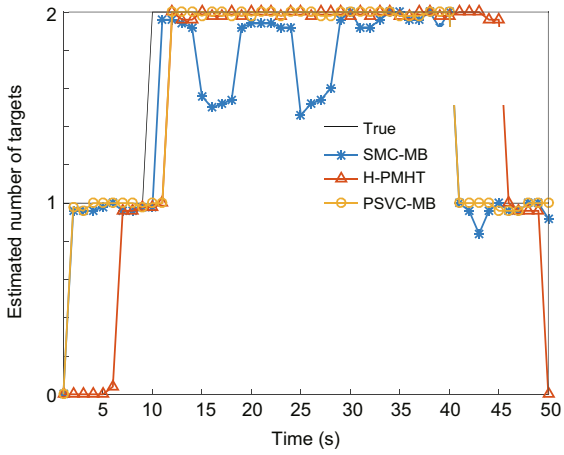

Fig. 8 Estimated number of targets of three different algorithms

Table 4 Target parameter setting when the targets are close to each other

Target index	Survival time (s)	Initial state
1	1–40	[19 pixels, 0.2 pixel/s, 14.7 pixels, 0.2 pixel/s]
2	10–50	[28.3 pixels, −0.1 pixel/s, 15.4 pixels, 0.2 pixel/s]

the particles become too compact, the density detector step will stop the position scaling step and the particles will move freely. Therefore, the looseness of particles is similar at high and low SCRs in the proposed algorithm.

Table 4 shows the target parameters when the targets are close to each other. Fig. 10 shows the true and estimated tracks of the proposed PSVC-MB algorithm with different SCRs.

When the targets are close to each other, the target influence areas overlap, and the amplitude of the corresponding resolution cell is very large. The algorithm proposed in this study can deal with the above problems well. It can be seen from Fig. 10 that the proposed algorithm can track accurately with different SCRs. Simultaneously when the targets are close, the estimated states will not be affected by the high amplitude. The estimated trajectory will not stay at the location of the high-amplitude resolution cell for a long time, and will not be confused with other target trajectories.

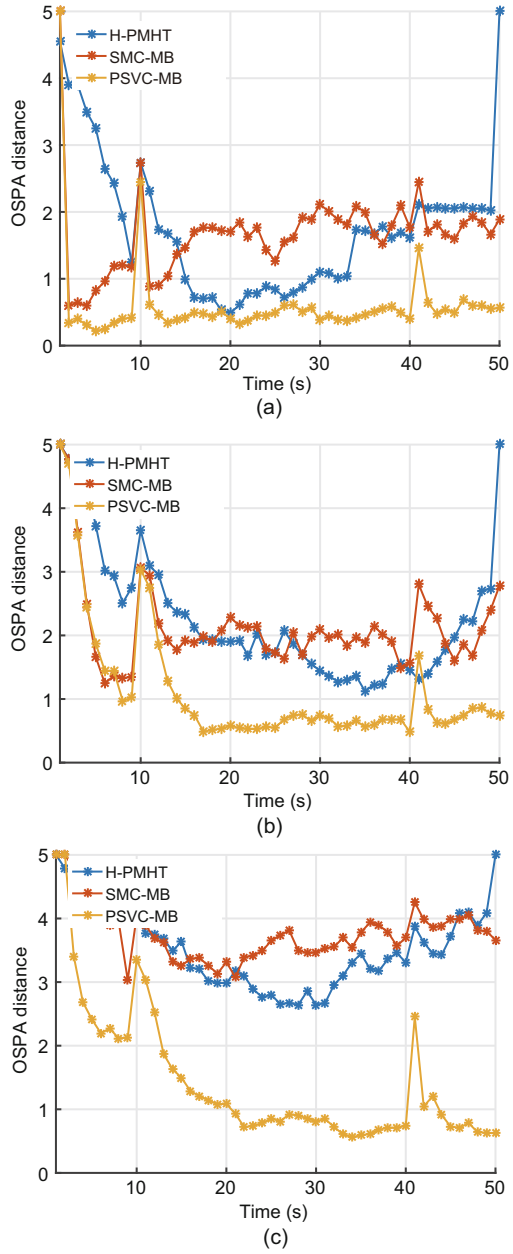

Fig. 9 The average OSPA distance of three different algorithms with different SCRs: (a) 9 dB; (b) 6 dB; (c) 4 dB

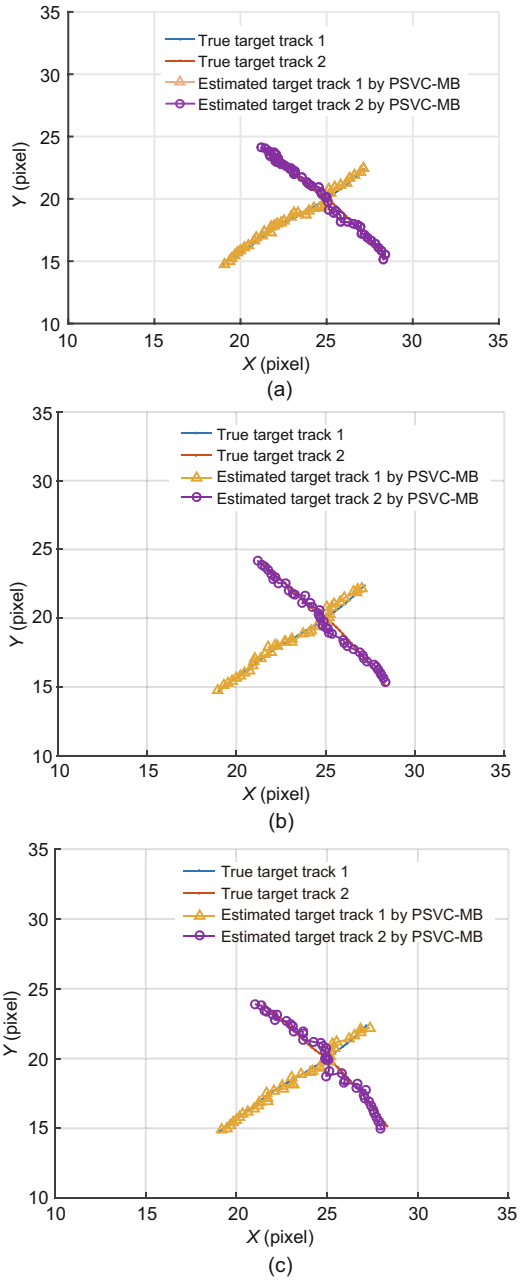

Fig. 10 Target tracks of PSVC-MB with different SCRs: (a) 9 dB; (b) 6 dB; (c) 4 dB

5 Conclusions

In this paper, a PSVC-MB algorithm is proposed to track maritime dim targets. The proposed algorithm uses the particle scaling method instead of the resampling method in the MB algorithm to solve the particle scarcity problem. In addition, the velocity correction and re-estimation algorithm is used to constrain the particle velocity. This method effectively solves the diffusion caused by random particle motion, increases the number of effective particles, and improves the tracking accuracy. In the simulations, the proposed PSVC-MB algorithm is compared with the SMC-MB and H-PMHT algorithms, and the results verify the effectiveness of the proposed algorithm.

Contributors

Yunfei GUO designed the research. Liwei SHI drafted the paper. Wenxiong CUI, Yanbo XUE, and Yun CHEN

helped organize the paper. Yunfei GUO and Liwei SHI revised and finalized the paper.

Conflict of interest

All the authors declare that they have no conflict of interest.

Data availability

The data that support the findings of this study are available from the corresponding author upon reasonable request.

References

Abraham DA, Lyons AP, 2002. Novel physical interpretations of K-distributed reverberation. *IEEE J Ocean Eng*, 27(4):800-813. https://doi.org/10.1109/JOE.2002.804324

Armstrong BC, Griffiths HD, 1991. CFAR detection of fluctuating targets in spatially correlated K-distributed clutter. *IEE Proc F Radar Signal Process*, 138(2):139-152. https://doi.org/10.1049/ip-f-2.1991.0020

Chesser JA, Nguyen HV, Ranasinghe DC, 2022. The Megopolis resampler: memory coalesced resampling on GPUs. *Dig Signal Process*, 120:103261. https://doi.org/10.1016/j.dsp.2021.103261

Davey SJ, Rutten MG, 2007. A comparison of three algorithms for tracking dim targets. Information, Decision and Control, p.342-347. https://doi.org/10.1109/IDC.2007.374574

Davey SJ, Gaetjens HX, 2018. Track-Before-Detect Using Expectation Maximisation—The Histogram Probabilistic Multi-Hypothesis Tracker: Theory and Applications. Springer, Singapore. https://doi.org/10.1007/978-981-10-7593-3

Ester M, Kriegel HP, Sander J, et al., 1996. A density-based algorithm for discovering clusters in large spatial databases with noise. Proc 2nd Int Conf on Knowledge Discovery and Data Mining, p.226-231.

Guo YF, Teng K, Shi LW, 2023. SA-HPMHT for maritime dim targets tracking with sensor location uncertainty. *IEEE Sens J*, 23(5):5134-5145. https://doi.org/10.1109/JSEN.2023.3238401

Kim DY, Ristic B, Wang XZ, et al., 2019. A comparative study of track-before-detect algorithms in radar sea clutter. Int Radar Conf, p.1-6. https://doi.org/10.1109/RADAR41533.2019.171306

Kim DY, Ristic B, Guan R, et al., 2021. A Bernoulli track-before-detect filter for interacting targets in maritime radar. *IEEE Trans Aerosp Electron Syst*, 57(3):1981-1991. https://doi.org/10.1109/TAES.2021.3054715

Li WJ, Yi W, Kong LJ, et al., 2022. An efficient track-before-detect for multi-PRF radars with range and Doppler ambiguities. *IEEE Trans Aerosp Electron Syst*, 58(5):4083-4100. https://doi.org/10.1109/TAES.2022.3158633

Liang MC, Kropfreiter T, Meyer F, 2023. A BP method for track-before-detect. *IEEE Signal Process Lett*, 30:1137-1141. https://doi.org/10.1109/LSP.2023.3296874

Moyer LR, Spak J, Lamanna P, 2011. A multi-dimensional Hough transform-based track-before-detect technique for detecting weak targets in strong clutter backgrounds. *IEEE Trans Aerosp Electron Syst*, 47(4):3062-3068. https://doi.org/10.1109/TAES.2011.6034689

Papi F, Vo BN, Vo BT, et al., 2015. Generalized labeled multi-Bernoulli approximation of multi-object densities. *IEEE Trans Signal Process*, 63(20):5487-5497. https://doi.org/10.1109/TSP.2015.2454478

Posner FL, 2002. Spiky sea clutter at high range resolutions and very low grazing angles. *IEEE Trans Aerosp Electron Syst*, 38(1):58-73. https://doi.org/10.1109/7.993229

Reuter S, Vo BT, Vo BN, et al., 2014. The labeled multi-Bernoulli filter. *IEEE Trans Signal Process*, 62(12):3246-3260. https://doi.org/10.1109/TSP.2014.2323064

Ristic B, Arulampalam S, Gordon N, 2004. Beyond the Kalman Filter: Particle Filters for Tracking Applications. Artech House, London, UK.

Ristic B, Vo BT, Vo BN, et al., 2013. A tutorial on Bernoulli filters: theory, implementation and applications. *IEEE Trans Signal Process*, 61(13):3406-3430. https://doi.org/10.1109/TSP.2013.2257765

Ristic B, Rosenberg L, Kim DY, et al., 2020. Bernoulli track-before-detect filter for maritime radar. *IET Radar Sonar Navig*, 14(3):356-363. https://doi.org/10.1049/iet-rsn.2019.0480

Ristic B, Kim DY, Rosenberg L, et al., 2022. Exploiting Doppler in Bernoulli track-before-detect for a scanning maritime radar. *IEEE Trans Aerosp Electron Syst*, 58(1):720-728. https://doi.org/10.1109/TAES.2021.3098117

Tian MC, Chen ZM, Wang HF, et al., 2022. An intelligent particle filter for infrared dim small target detection and tracking. *IEEE Trans Aerosp Electron Syst*, 58(6):5318-5333. https://doi.org/10.1109/TAES.2022.3169447

Vo BN, Vo BT, Pham NT, et al., 2010. Joint detection and estimation of multiple objects from image observations. *IEEE Trans Signal Process*, 58(10):5129-5141. https://doi.org/10.1109/TSP.2010.2050482

Vu HX, Davey SJ, Arulampalam S, et al., 2013. H-PMHT with a Poisson measurement model. Int Conf on Radar, p.446-451. https://doi.org/10.1109/RADAR.2013.6652030

Ward K, Tough R, Watts S, 2013. Sea clutter: scattering, the K distribution and radar performance. *Waves Random Compl Med*, 17(2):233-234. https://doi.org/10.1080/17455030601097927

Xu C, He ZS, Liu HC, et al., 2021. Bayesian track-before-detect algorithm for nonstationary sea clutter. *J Syst Eng Electron*, 32(6):1338-1344. https://doi.org/10.23919/JSEE.2021.000113

Yi W, Morelande MR, Kong LJ, et al., 2013. An efficient multi-frame track-before-detect algorithm for multi-target tracking. *IEEE J Sel Top Signal Process*, 7(3):421-434. https://doi.org/10.1109/JSTSP.2013.2256415